Lithosphere

Research Article

An Integration Method of Bursting Strain Energy and Seismic Velocity Tomography for Coal Burst Hazard Assessment

Jinzheng Bai [ID],[1] **Linming Dou** [ID],[1] **Wu Cai** [ID],[1] **Siyuan Gong** [ID],[1,2] **Wei Shen** [ID],[3] **Xinyuan Tian**,[1] **and Hongjun Ma**[4]

[1]*State Key Laboratory of Coal Resources and Safe Mining, School of Mines, China University of Mining and Technology, Xuzhou, Jiangsu 221116, China*
[2]*China University Mining & Technology, School of Mines, Jiangsu Engineering Laboratory Mine Earthquake Monitoring & Prevention, Xuzhou, Jiangsu 221116, China*
[3]*Huaiyin Institute of Technology, Faculty Architecture & Civil Engineering, Huai'an, Jiangsu 223001, China*
[4]*Kailuan (Group) Coal Industry Co Ltd, Tangshan, Hebei 063000, China*

Correspondence should be addressed to Wu Cai; caiwu@cumt.edu.cn

The occurrence of coal burst in underground coal mines is complex, abrupt, and diverse, and the evaluation and prediction of coal burst hazard is the premise of effective prevention and control of coal burst. In this study, a coal burst carrier system model under the synergistic action of roof, coal seams, and floor was established, and the evolution of coal burst in underground coal mines was discussed based on the stress-vibration-energy coupling principle. On this basis, an integration method of bursting strain energy and seismic velocity tomography for coal burst assessment was proposed. With the deep and complex panel in a mine as the research object, the coal burst risk of the panel during excavation was evaluated in time and space domains, respectively. Results showed that the bursting strain energy and the active seismic velocity tomography technology can accurately identify both the positive anomalies and the negative anomalies of stress field and energy field in the mining period. Moreover, the method can not only evaluate the coal burst risk of the panel in the temporal domain but also predict the area with potential strong seismic events in the spatial domain. The research conclusions can accurately illustrate the whole complex evolution process of coal burst in underground coal mines.

1. Introduction

Coal burst refers to the sudden, rapid, and violent release of elastic deformation energy accumulated in coal or coal measure rocks triggered by coal mining, thus causing strong vibration, casualties, equipment destruction, roadway failure, and dust explosion [1, 2]. In China, as recent years have witnessed a rising mining depth and mining intensity, underground mining space is faced with unprecedented high-stress environment and complex mining layout. Accordingly, the frequency and intensity of coal burst accidents have also jumped, and coal burst has become one of the most severe dynamic disasters threatening deep coal mining [3–5]. How to break through the technical limits of

poor underground exploration and opaque geology of the mining space and realize the evaluation and prediction of coal burst hazards is an important topic in the accurate prevention and control of coal burst.

In recent years, a growing number of theories and technologies based on geophysical methods to evaluate coal burst hazard have been widely in underground mines used for coal burst assessment. Representative studies include as follows: Srinivasan et al. believed that the total frequency $\sum N$ and total energy $\sum E$ of microseismic events in a fixed time window could predict seismic events in the future [6]. Gutenberg and Richter et al. held that a significant decrease in b value agreed well with an increase in the number of strong seismic events [7, 8]. Cao and Cai et al. continuously
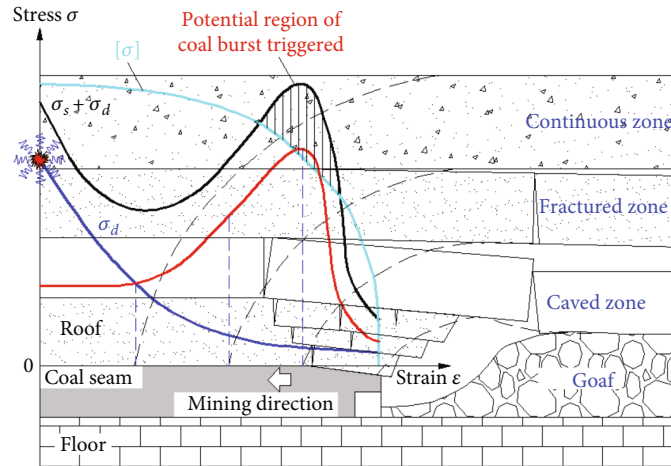
FIGURE 1: Schematic diagram of coal burst induced by the superposition of static and dynamic stresses.

monitored the relatively high-stress areas of coal mine panel by the passive tomography technology and then evaluated the burst hazard of the panel [9, 10]. He et al. investigated the rock burst (including the source location, energy, damage range, and modes of ensuing damage) and the temporal and spatial evolution laws of the monitoring parameters of microseismic (MS) and acoustic emissions (AE) [11]. Based on the bed separation telemetry and electromagnetic radiation, Zhao et al. proposed the long-term and short-term prediction model of rock burst in coal seam with hard roof [12]. Zhang et al. proposed comprehensive weight and extension methods to research the rockburst prediction [13]. By linking stress, strain, damage, and microseismic energy release, Cai et al. proposed a new index called "bursting strain energy (BSE)" to quantitatively evaluate the bursting hazard of coal, which is a useful tool to quickly identify and analyze the stress distribution and the anomaly degree of burst hazard [14, 15]. Feit et al. developed a method for estimating the outburst and rock burst hazard of coal seams and faces of mine workings on the basis of determination of rock-mass energy [16].

From the perspective of mechanics, the whole process (incubation, triggering, and disaster) of coal burst is essentially a process of deformation, damage, and failure (instability) of the seismogenic body under the action of force, which is basically consistent with the deformation and fracture process of loaded coal and rock mass [17, 18]. Considering that the occurrence of coal burst are subject to complex and different influencing factors which are coupled with each other, the precursory information of coal burst induced by different geological and mining conditions might differ. Resultantly, a single evaluation index and method can merely describe the hazard of coal burst from one perspective, failing to fully reflect the spatially multidimensional information that induces coal burst. Previous research results mainly focused on single mining-induced stress, vibration, or energy. The single index proposed on this basis can hardly be further improved after its prediction efficiency reaches a certain degree. Therefore, it is necessary to quantitatively evaluate the coal burst hazard during the mining process of panels under complex mining conditions from a comprehensive perspective of mining-induced stress, vibration, and energy.

In this study, the evolution process of coal burst in underground coal mine based on the stress-vibration-energy coupling principle was discussed. Furthermore, a detection scheme integrating the active seismic velocity tomography (SVT) technology and the BSE was proposed. With a deep and complex panel as the research object, the whole process of burst hazard of the panel was evaluated in time and space domains, respectively. The research conclusions can ensure the safety and prevent coal burst hazard in deep and complex working face.

2. Internal Mechanism and Methods

2.1. Interpretation of Coal Burst Process Based on the Stress-Vibration-Energy Coupling Principle. As shown in Figure 1, during the mining of the underground longwall panel, the static stress environment of the coal and rock mass in front of the working face is in an originally quasi hydrostatic pressure state. Under mining disturbance, the vertical stress (i.e., abutment pressure) in the coal seam gradually increases to the peak stress; then it enters the pressure-relief state with the damage of the coal body and finally decreases to the unidirectional residual strength state at the coal wall of the working face.

In underground mining, the stress response of coal and rock mass to mining activities is reflected by the dynamic load of mining disturbance (such as coal cutting, support moving, mechanical vibration, blasting, roof and floor breakage, instability of coal and roof structure, gas outburst, coal blasting, fault, and slip); it is then superimposed with the abutment stress (static load) of the coal body around the stope and roadway. Once the superimposition exceeds the bearing limit of the coal body, coal and rock dynamic disasters are likely to occur [19]. The mechanism of coal burst induced by the superposition of dynamic and static loads can be expressed by
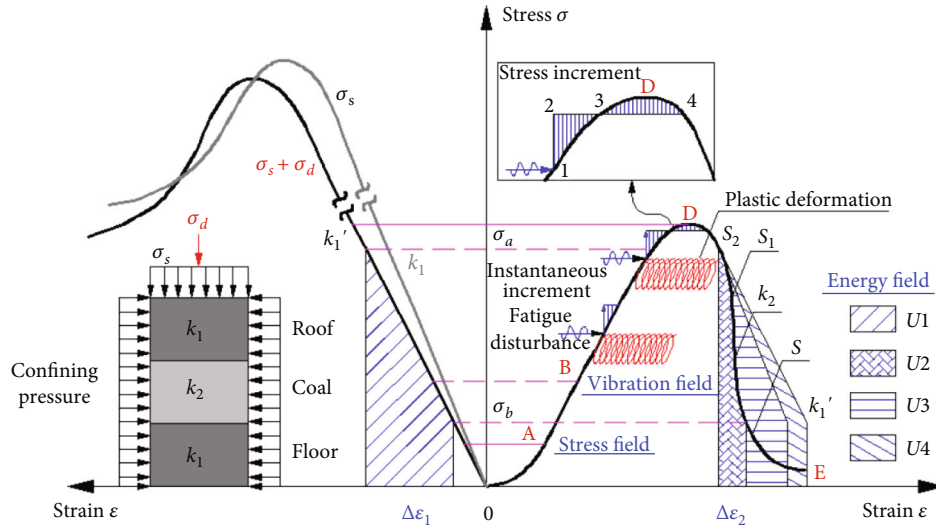
$$\sigma_s + \sigma_d \geq \sigma_{b\ \min}, \tag{1}$$

FIGURE 2: Stress-energy principle of coal burst process [21, 22].

where σ_s is the static load stress of coal and rock mass, σ_d is the dynamic load stress of mining disturbance, and $\sigma_{b\,min}$ is the critical stress of coal burst.

The model of the coal burst carrier system is composed of a roof, a coal seam, and a floor (Figure 2). The roof and floor, which can be regarded as complete surrounding rock, have a much greater stiffness and strength than the coal seam. The loaded stress-strain relationship of roof and floor is described by the left curve, while that of the coal body in front of the panel is described by the right curve. In Figure 2, $U1$ is the released elastic energy of the surrounding rock during bursting; $U2$ is the consumption of the released elastic energy of the surrounding rock by the coal seam during bursting; $U3$ is the residual elastic energy released by the whole system during bursting; $U4$ is the additional input energy.

According to the mechanism of coal burst induced by the superposition of dynamic and static loads under the influence of the mining-induced quasi-static load (σ_s) [20], when the coal seam generates a strain increment ($\Delta\varepsilon_2$), the corresponding strain increment ($\Delta\varepsilon_1$) generated by the surrounding rock of the roof and floor is

$$\Delta\varepsilon_1 = \frac{k_2}{k_1}\Delta\varepsilon_2, \qquad (2)$$

where k_1 and k_2 are the stiffnesses of the surrounding rock and the coal seam, respectively. The total strain increment ($\Delta\varepsilon$) generated by the whole system of roof-coal seam-floor is

$$\Delta\varepsilon = \Delta\varepsilon_1 + \Delta\varepsilon_2 = \frac{k_1 + k_2}{k_1}\Delta\varepsilon_2, \qquad (3)$$

where the ratio of the strain increment of the coal seam to the strain increment of the whole surrounding rock system is

$$\frac{\Delta\varepsilon_2}{\Delta\varepsilon} = \frac{1}{1 + (k_2/k_1)}. \qquad (4)$$

The conversion of microseism-stress-strain energy in the failure process of the whole roof-coal seam-floor coal burst carrier system can be expressed by the following equation, and its criterion is $U3 > 0$. Thus, the released energy of microseism is directly proportional to the squares of the stress drop and strain increment.

$$U3 = U1 - U2 \approx -\frac{k_1 + k_2}{2k_1}\cdot(\sigma_a + \sigma_b)\cdot\Delta\varepsilon_2 = \frac{k_1 + k_2}{2k_1\cdot k_2}\cdot(\sigma_a^2 - \sigma_b^2), \qquad (5)$$

$$E = \eta\cdot U3 = \frac{\sigma_a - \sigma_b}{\sigma_a + \sigma_b}\cdot U3 \propto (\sigma_a - \sigma_b)^2 \propto (\Delta\varepsilon)^2, \qquad (6)$$

where σ_a and σ_b are stress before and after coal burst, $\Delta\varepsilon_2$ is indicated in Figure 2, and E and η are the microseismic energy and efficiency, respectively.

With reference to Figure 2 and Equations (4) and (6), the force in the whole process of coal burst evolution (incubation-triggering-appearance-end) can be explained as follows:

2.1.1. AB Stage. Both k_1 and k_2 are above 0 and remain unchanged, so $k_1 + k_2 > 0$; the value of $\Delta\varepsilon_2/\Delta\varepsilon$ also remains unchanged. The surrounding rock (i.e., the roof and floor F) and the coal seam are in the elastic energy storage stage, which belongs to the incubation stage of coal burst.

2.1.2. BD Stage. k_2 gradually decreases to 0, and k_1 remains the same; moreover, $k_1 + k_2 > 0$. The value of $\Delta\varepsilon_2/\Delta\varepsilon$ rises with the decrease in the value of k_2/k_1; the surrounding rock of roof and floor continues to accumulate elastic energy, but the coal body begins to experience plastic deformation. At this stage, microcracks begin to emerge, incubate, and expand in the coal body, resulting in the phenomena of microseism/acoustic emission. This is the precursory stage of coal burst.

2.1.3. DS₁ Stage. k_2 is less than 0 and gradually decreases, while k_1 remains unchanged; currently, $k_1 + k_2 \geq 0$ and $U3 \leq 0$. When $k_1 + k_2 = 0$, it corresponds to point S_1 in Figure 2; meanwhile $\Delta\varepsilon_2/\Delta\varepsilon \longrightarrow \infty$, corresponding to the triggering moment of coal burst.

2.1.4. S₁E Stage. k_2 is below 0, and it decreases first and then increases. k_1 remains unchanged, and the state changes from $k_1 + k_2 < 0$ ($U_3 > 0$) to $k_1 + k_2 > 0$ ($U_3 < 0$); as the value of k_2/k_1 decreases first and then increases, the value of $\Delta\varepsilon_2/\Delta\varepsilon$ rises first and then declines, corresponding to the stage from the appearance of coal burst to the end.

2.2. Active SVT Technology. Numerous studies show that a coal burst may occur when the stress within coal-rock mass reaches a certain critical stress level [23, 24]. Velocity tomography technology relies on the propagation law of seismic waves, especially P-waves in a rock mass to determine the relative state and stress redistribution of the rock mass. It boasts a wide detection range and high accuracy; moreover, it does not damage the target area. High-velocity and low-velocity areas in a homogeneous rock mass indicate rising stress and falling stress, respectively [25–27]. According to the types of generating sources, velocity tomography can be divided into active velocity tomography and passive velocity tomography [28, 29]; the former uses vibrators, such as hammering, blasting, equipment, and cutting, while the latter takes the microseismic events induced by mining as the triggering sources of seismic waves. Studies have proven that the active velocity tomography technology is more reliable in areas that require high detection accuracy of stress distribution [30, 31]. The essence of active SVT to solve the stress field distribution in a mining area lies in finding an optimal wave velocity field to minimize the difference between the calculated wave velocity and the recorded one. The arrival time of the calculated vibration wave can be expressed by [32]:

$$t_i = \int_{\Gamma_i} \frac{1}{V(x,y,z)} d\vec{x} t_0 = \int_{\Gamma_i} S(x,y,z) d\vec{x} + t_0, \qquad (7)$$

where $V(x,y,z)$ is the velocity field of the vibration waves, m/s; t_i is the arrival time of the calculated vibration waves, s; t_0 is the triggering moment of the active source, s; and Γ_i is the ray path; $S(x,y,z) = 1/V(x,y,z)$ is the slowness field of the vibration waves, s/m.

An initialization wave velocity model of three-dimensional grid based on the mining area that shall be detected is established. In the model, the propagation time of the i-th ray is

$$t_i = \sum_{j=1}^{M} S_j d_{ij} + t_0 (i = 1, \cdots N), \qquad (8)$$

where d_{ij} is the length of the i-th ray passing through the j-th grid; S_{ij} is the slowness of the i-th ray propagating in the j-th grid; and M and N are the total numbers of grids and rays, respectively. Thus, an equation system including N equations and M variables was established, which might be underdetermined or overdetermined. Synchronous iterative reconstruction technology (SIRT) is considered an effective method to solve and operate the equation system [33].

The prediction of coal burst hazard is based on the determination of the stress state and stress concentration degree in coal and rock strata. Generally, in areas with a high stress level and high concentration degree, positive anomalies of P-wave velocity are more notable than in other areas. To further quantitatively evaluate the burst hazard reflected by the active SVT, an evaluation index (An) for wave velocity anomaly was proposed. The relationship between the positive anomaly of wave velocity and the degree of stress concentration is shown in Table 1. It is calculated as follows:

$$A_n = \frac{v_p - v_p^a}{v_p^a}, \qquad (9)$$

where v_p is P-wave velocity of a certain point and v_p^a is the average velocity of the model.

2.3. BSE Index. Coal burst is caused by strain energy released from the surrounding rock, plus the additional energy input provided by the superposition of static and dynamic stresses [34, 35]. According to the continuum damage mechanics, the stress in the loaded coal can be described by

$$\sigma = E\varepsilon(1 - D), \qquad (10)$$

where σ is the stress, MPa; ε is the strain; E is the Young's modulus, GPa; and D is the damage variable.

To establish relationships between the redistributed stress based on the on-site microseismic monitored data and the dynamic and static load stresses of the coal burst carrier system in Figures 1 and 2, the damage variable defined with reference to the Benioff strain [36] is as follows:

$$D = 1 - \exp\left(-\frac{\varepsilon E}{\varepsilon F}\right), \qquad (11)$$

where $\varepsilon E = \sum \sqrt{U_{SE}}$ is the cumulative Benioff strain; εF is the average value of εE, which can be determined by assuming that the complete damage state corresponds to the critical damage ($D = 0.95$). DF and εEF are substituted into Equation (11) to calculate εF:

$$\varepsilon F = -\frac{\varepsilon EF}{\ln(1 - DF)}. \qquad (12)$$

Equation (12) is substituted into Equation (11); then the redistributed stress can be obtained:

$$\sigma I = E\varepsilon \exp\left(-\frac{\varepsilon E}{\varepsilon F}\right). \qquad (13)$$

TABLE 1: Relationship between positive anomaly in wave velocity and stress concentration.

Coal burst hazard	Stress concentration	Positive velocity anomaly, an (%)	Stress concentration probability
0	None	<5	<0.2
1	Weak	5 ~ 15	0.2~0.6
2	Moderate	15 ~ 25	0.6~1.4
3	Strong	>25	>1.4

Therefore, a new BSE index is defined [14]:

$$\text{BSE} = \begin{cases} 1 - \left| D - \dfrac{\sigma I}{\sigma P} \right|, \\ D, \end{cases} \qquad (14)$$

where $0 \le \text{BSE} \le 1$; σP is the peak value of the redistributed stress. To apply this index to on-site coal burst hazard prediction, this index is defined as four different prediction levels (i.e., 0-0.25, 0.25-0.5, 0.5-0.75, and 0.75-1), corresponding to four coal burst hazard levels (i.e., none, weak, moderate, and strong). As shown in Table 2, different coal burst control measures can be taken according to the index value. BSE is explored, redistributed, and extracted from the on-site basic microseismic data reflecting the vibration field of coal and rock mass. Considering both this fact and the evolution of the energy field of the whole coal burst process (from incubation, triggering, appearance to end), BSE can reflect the seismic field and energy field of coal and rock mass. The rationality of this index is verified by field application.

3. Field Application

3.1. Site Description. The 0250 fully mechanized longwall panel (hereafter referred to as Panel 0250) is the third panel of the No. 5 coal seam of the South No. 5 mining area of a deep mine in Hebei Province, China. According to Figure 3(a), parameters of Panel 0250 are as follows: the dip length of 150 m, the strike length of 568 m, the average thickness of the coal seam of 2.8 m, the average dip angle of 20°, and the buried depth of the coal seam is about 697 m-835 m. From south to north, the northwest side of the panel is Goafs T_1450, T_1453, T_1452, and T_1451, respectively; the east side is Goafs 0251 and 0253, and the lower part of the middle part of the panel is Goaf 0290. There are two interior key strata and one main key stratum above the No. 5 coal seam in Panel 0250 (Figure 3(b)). The three strata are medium sandstone, siltstone, and siltstone with thicknesses of 6.98 m, 13.99 m, and 22.98 m, respectively, and they are 0 m, 6.98 m, and 78.69 m away from the No. 5 coal seam, respectively. According to the measurement of physical and mechanical parameters, the coal seam and its roof and floor in the No. 8 and No. 9 seams are prone to coal burst. According to Figure 3(c), there are 9 faults (F_1-F_9) in the panel, four of which (i.e., F_6, F_7, F_8, and F_9) expose the panel roadway, exerting a significant impact on excavation.

As shown in Figure 4, an MS microseismic monitoring system was installed in the Panel 0250. Microseismic sensors, which could capture the location and energy level of microseismic signals in the mining process and realize a real-time monitoring of the vibration field and energy field of the panel, were arranged in the centralized roadway on Panel 0250 and its northwest side.

3.2. Assessment Scheme of the Active SVT Technology. For monitoring the stress field of Panel 0250, active SVT detection was carried out in Nov. 2019. The portable distributed test system (GeoPen SE2404NTM three-dimensional telemetry seismic acquisition system) was composed of a main control unit, a data acquisition station, a cross station, an instantaneous detonator, data transmission composite cables, a geophone, and a remote blasting decoder. The frequency range was 225-233 MHz/7 W/16 channel, and the data flow port was 1 Mbps. The system was connected in series (Figure 5(a)). The construction and subsequent analysis are shown in Figure 5(b). In this detection, 60 signal receiving points were set at the chute of Panel 0250, with a spacing of 10 m; a total of 75 blasting shots were set in the air duct of Panel 0250 with a spacing of 8 m. The parameters (sampling frequency of 5,000 Hz, the number of sampling points of 8 k, and the single recording time length of 1.6 s) meet the requirements of complete record of waveforms.

Among the 75 active vibration signals that were excited in the detection, only 70 signals were successfully received due to underground noise, humidity, and equipment instability. After preliminary screening, 2,048 effective waveforms were reserved. The formed ray group can well cover the whole panel to ensure the accuracy and reliability of the detection results.

The arrival time of the first wave of the collected waveforms were marked in turn by the GeoWave software. Most waveforms were clear, which helped to accurately identify the arrival time of the first wave. Considering that the active signals were excited by a single detonator and obvious delay occurred between the initiation times of different active sources, the delay error determined to be 6.96 ms by the minimum two division method. The velocity of the first wave was distributed in the range of 3.13-4.12 km/s, and a uniform wave velocity model whose initial wave velocity was 3.6 km/s was established. The propagation path of the active source in the middle of coal and rock was determined by the straight ray tracing method. To improve the calculation efficiency, the numbers of grids in the X, Y, and Z directions are $30 \times 103 \times 4$, the grid size being $6\,\text{m} \times 6\,\text{m} \times 137\,\text{m}$. A total of 15 rounds of cyclic inversion were performed with the aid of the SIRT, and the current slowness was adjusted and modified in each calculation cycle until the remaining time became acceptable or the number of iterations reached the threshold.

3.3. Periodic Detection of BSE. Based on long-term theoretical research, laboratory tests, and field tests, it is concluded that the mechanism of the whole coal burst process of

TABLE 2: Relationship between the BSE index value range, the coal burst risk level, and the corresponding guidelines on coal burst control measure.

| BSE index value range	Coal burst hazard level	Control measures
0 ≤ BSE<0.25	None	All mining operations can be carrying out normally
0.25 ≤ BSE<0.50	Weak	More attention should be focused on monitoring and forecasting of coal burst in the process of mining operations
0.50 ≤ BSE<0.75	Moderate	Stress relief measures should be taken to alleviate and eliminate the coal burst risk in the process of mining operations
0.75 ≤ BSE<1	Strong	Production should be paused, and workers must be evacuated from the risk regions immediately. Further mining operations cannot be restored until the coal burst risk has been eliminated by taking the measures and being guaranteed again with the monitoring results
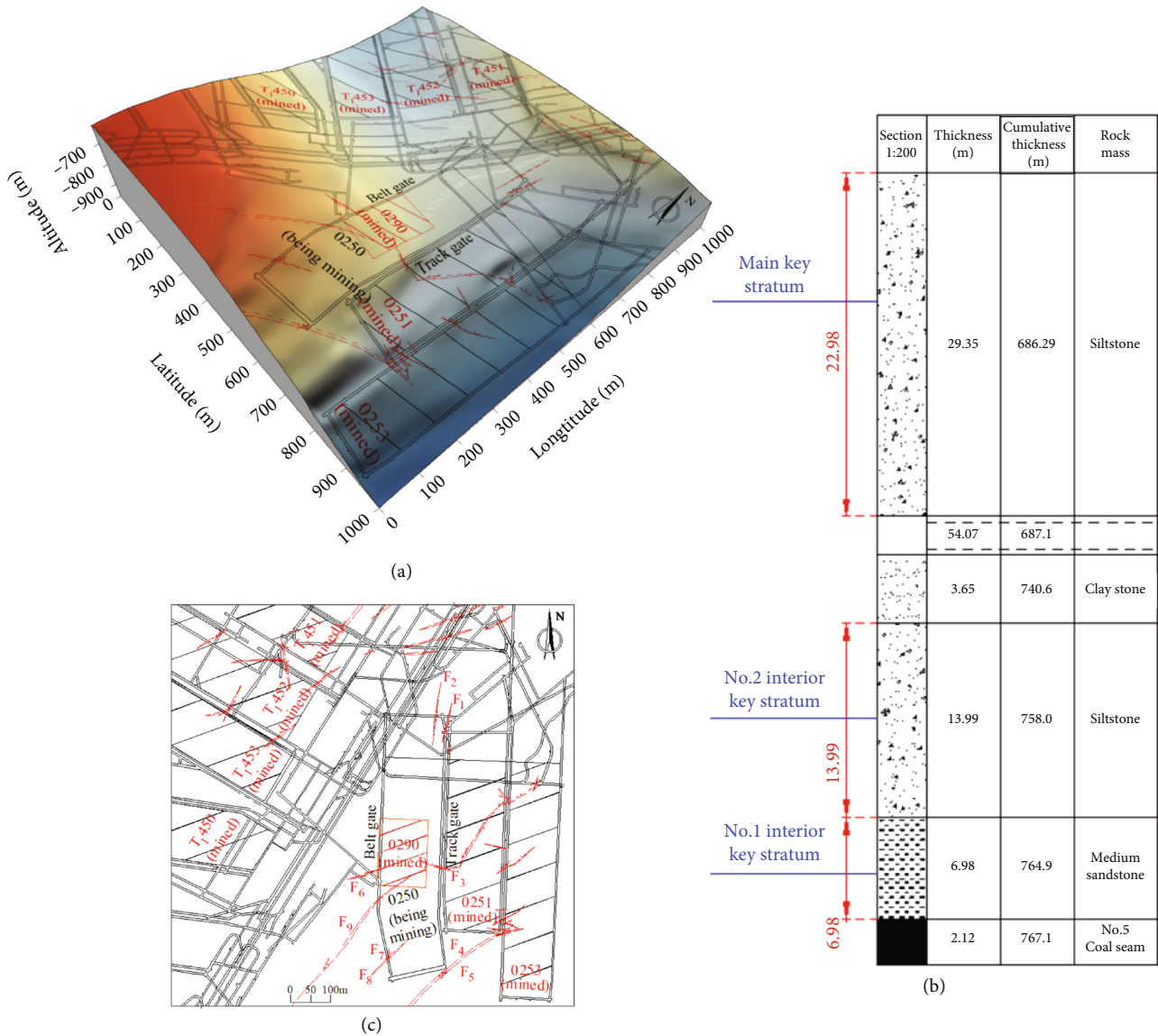
FIGURE 3: Mining engineering plan of Tangshan Coal Mine. The surface shows the coal seam floor. (a) Layout of LW 0250. (b) The overlay strata profile. (c) Geological structure near LW 0250.

"incubation-triggering-appearance-end" should meet three conditions (strength, energy, and coal burst proneness); the latter two are sufficient conditions, while the first is a neces-sary condition; that is, coal burst will not occur if the stress of the coal and rock mass does not exceed its strength [14]. Therefore, with reference to Figure 2, the determination of
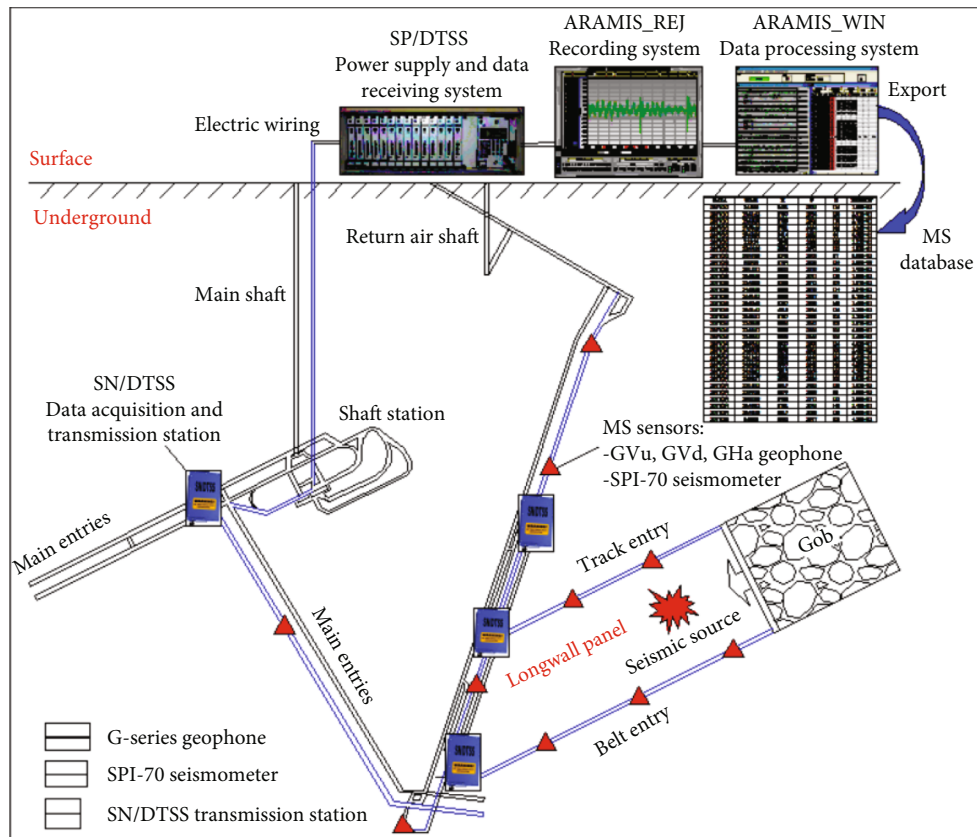
FIGURE 4: MS monitoring system in Tangshan coal mine.

the peak strength D point of the coal and rock mass is the key to accurately predict the occurrence of coal burst. Based on the MS microseismic monitoring system arranged in Panel 0250 (Figure 4), signals of fractures in the coal and rock mass during mining were collected as the data basis of BSE prediction index.

As shown in Figure 6(a), the excavation of Panel 0250 began in Dec. 2019 and ended in Jan. 2021. The mining was halted in Aug. and Sep. 2020 due to management factors. Its burst hazard was detected periodically monthly. Figure 6(b) shows the flow diagram to calculate the BSE. The burst hazard prediction based on BSE is divided into the time domain and the space domain. In field implementation, generally, 3-month historical microseismic data serve as the basic database for training to obtain hazardous seismic events and critical burst strain values, respectively. Then, the BSE index is obtained through normalization index processing.

4. Results and Discussion

4.1. Assessment Results of the Active SVT Technology. Figure 7(a) shows the wave velocity distribution of Panel 0250 with the aid of the active SVT technology. Obviously, the wave velocity of the whole panel is not evenly distributed. Instead, several obvious high-wave velocity anomaly areas (the wave velocity in the range of 2.0-6.5 km/s) can be observed, indicating that some areas are in the state of stress concentration and correspond to high coal burst haz-

ard. In contrast, some areas are in the state of stress-relief, corresponding to low burst hazard.

Specifically, there are three high-wave velocity zones (Zones A, B, and C) and one low-wave velocity zone (Zone D). The peak wave velocities in Zones A, B, and C reach 6.0 km/s, 5.2 km/s, and 6.5 km/s, respectively. All of them are positive anomaly zones of wave velocity. In contrast, the peak wave velocity in Zone D is merely 2 km/s, indicating a negative anomaly zone of wave velocity. This shows that the burst hazards follow the order: Zone C > Zone A > Zone B > Zone D, and the range of the wave velocity anomaly zones follow: Zone D > Zone A > Zone B > Zone C. Zone A is close to the side of open-off cut and chute and is obviously affected by the cutting of adjacent faults, such as F_6, F_7, F_8, and F_9. Zone B is on the goaf side of the single "square" stage, suggesting that roof suspension leads to a certain stress concentration. Zone C is close to the intersection of the stopping line and main roadway, and it is close to the "peninsula" coal pillar area formed by multi-face goafs, with high coal burst hazard. Zone D is located above the goaf of the underlying Panel 0290. As the lower No. 9 coal seam is mined, the stress is effectively released, displaying a good "unloading-pressure relief" effect and showed low coal burst hazard.

According to the research results, zones with potential burst hazard include high-wave velocity anomaly zones and anomaly zones that are witnessing the transformation from a high-wave velocity to a low=wave velocity. Those
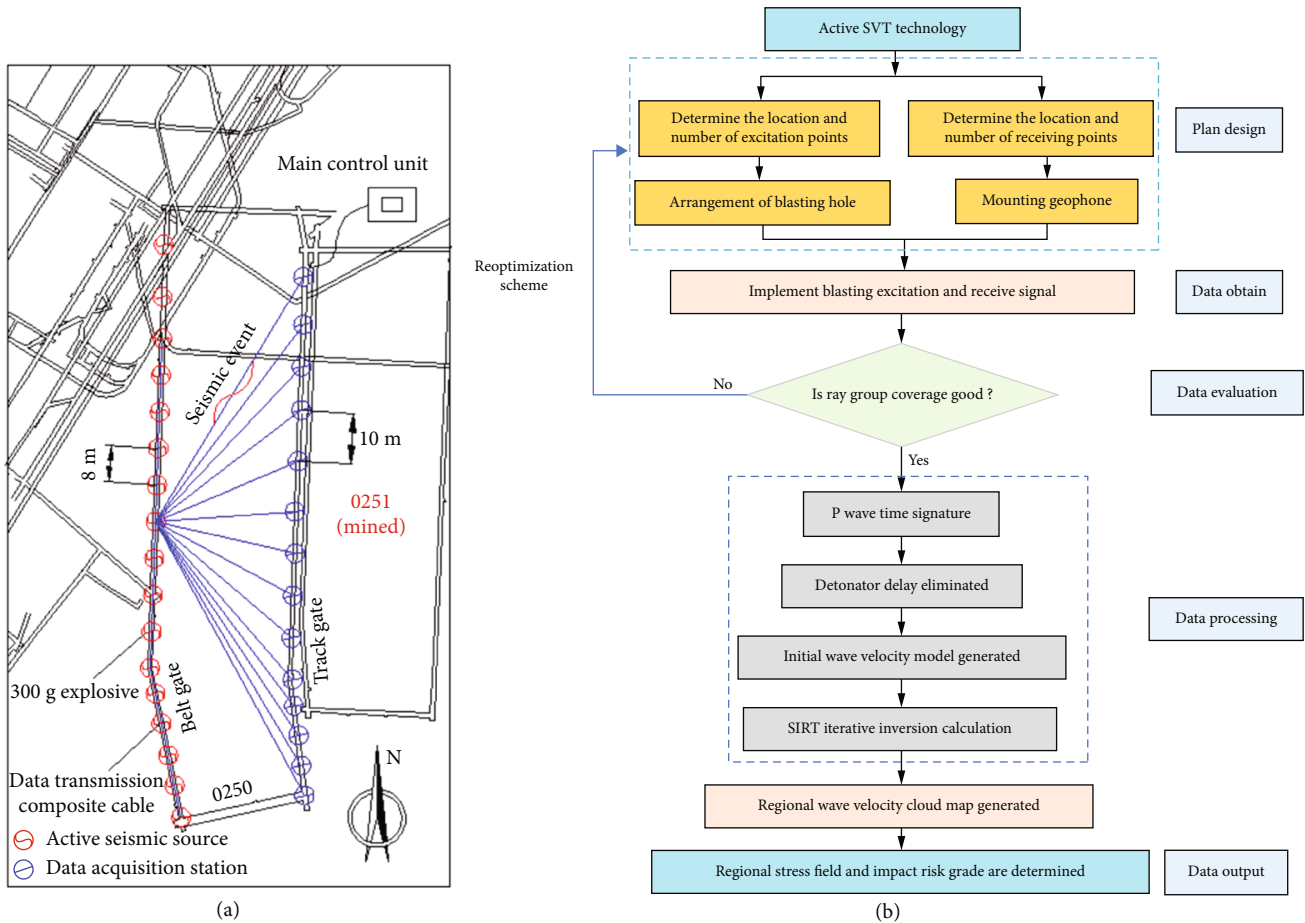
FIGURE 5: Illustration of equipment connection and construction process. (a) Illustration of equipment connection. (b) Assessment scheme of the active SVT technology.

wave velocity anomaly zones determined accordingly are the focus of monitoring and pressure relief in the excavation process.

According to the wave velocity anomaly coefficient *An*, the coal burst hazard clods is given in Figure 7(b). The wave velocity anomaly coefficients of Zones A, B, and C are 0.65, 0.45, and 0.85, respectively. They all reach the level of strong burst hazard. Before mining approaches these three zones, pressure-relief measures should be taken, such as large-diameter drilling in coal, roof blasting, and roof cutting. Mining can be resumed only after they reach the coefficient of safe stress concentration by effect verification. The wave velocity anomaly coefficient of Zone D reaches -0.40, the lowest coal burst hazard. Advancing excavation at a constant speed can prevent coal burst. Therefore, the stress-field-based active SVT technology can not only identify positive anomalies of stress field, but also accurately reflect its negative anomalies. And this evaluation result completely corresponds to the actual mining conditions on site.

4.2. Assessment Results of BSE. The process flow in Figure 6(b) was implemented for real-time continuous monitoring of the vibration field of Panel 0250 during mining. First, by regarding the 3-month historical database before

mining as the basic data, data training with 75% prediction efficiency was performed. With the aid of the linear correlation coefficient method proposed by Cai et al. [10], the complete damage state of the critical hazard seismic event was determined as 11,296 J, and the background value of the seismic event was 6,241 J. It was assumed that the coal and rock mass is completely damaged when D equals 0.95. Under such an assumption, the critical Benioff strain was determined, i.e., $\varepsilon F = 6{,}241 \, J^{1/2}$ and the correlation coefficient of strain and seismicity (α) was assumed 0.00072. The redistributed stress in the spatial domain was calculated. Figures 8(a)–8(i) give the nephrograms of spatial distribution of monthly BSE index during excavation in Panel 0250.

According to Figures 8(a)–8(c), like the detection results of active SVT, the BSE distribution near the panel at the initial stage of mining can be classified into different zones. The excavation of multiple roadways in the north of Panel 0250 was conducted in Dec. 2019, resulting in more concentrated BSE distribution in this area (a-A and b-A). Subsequently, the stress concentration weakened as the excavation ended. Faults F_6-F_9 were successively exposed on the side of the transportation trough during excavation. Mining disturbance broke the friction balance at the fault plane, leading to fault instability and rapid reduction of shear stress and
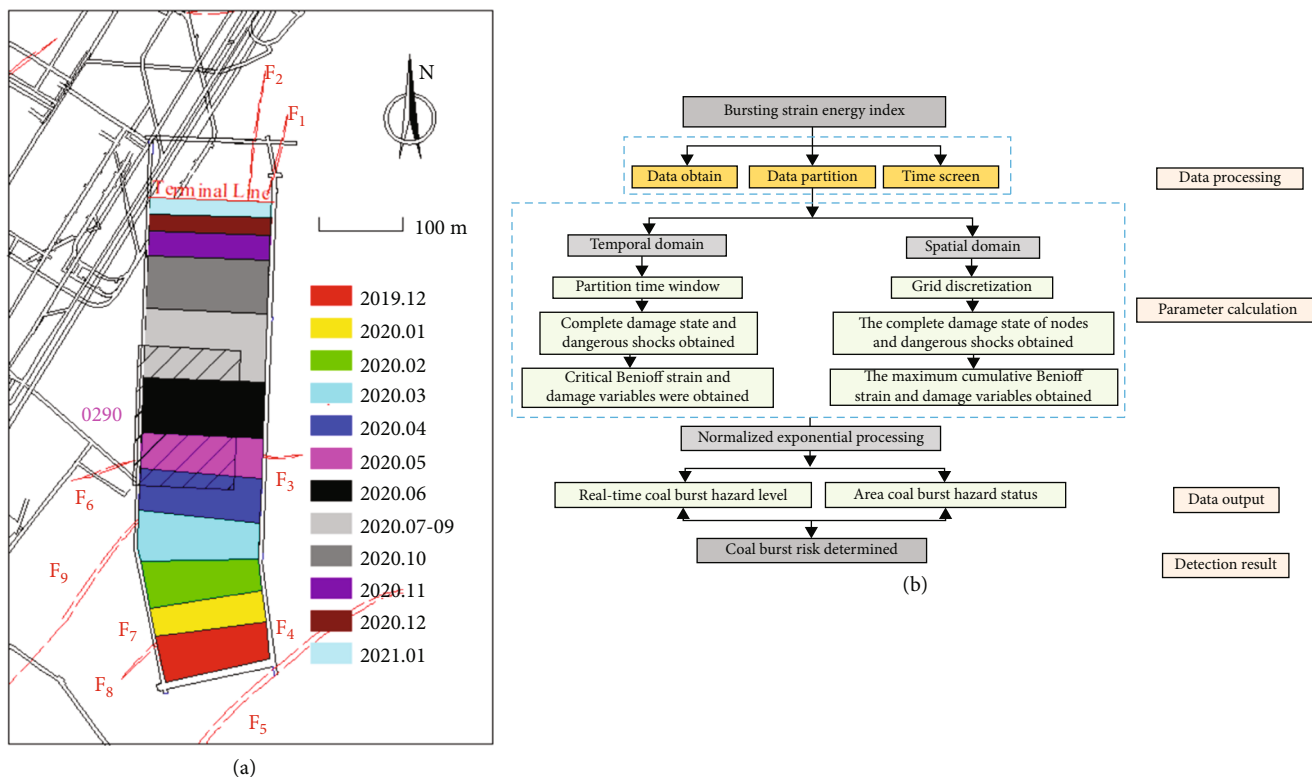
FIGURE 6: Excavation progress of the panel and calculation process of the BSE index. (a) Excavation progress of the panel. (b) Calculation process of the BSE index.

normal stress, as well as a sudden release of a large amount of accumulated elastic strain energy. In the early mining stage, the active SVT technology detected the existence of anomalies in the stress field of this area. Therefore, during excavation, a special pressure-relief measure of large-diameter drilling of the coal body was implemented on the solid coal side within 155 m of the air duct ahead of the panel (Zone A in Figure 8(n)). The specific parameters are as follows: the spacing of 1.5 m, the depth of over 20 m, and the diameter of 150 mm. The active pressure-relief measure results in a normal BSE distribution in this area (c-B). At this stage, the anomaly area of stress is mainly distributed near the fault outside the roadway, which has little impact on the coal burst hazard of the working face. This suggests that the detection method based on active SVT technology and BSE index can effectively guide pressure-relief measures.

As shown in Figure 8(d), at this time, the panel is approaching a "square" stage. The burst hazard inside the panel rises as a result of the frequent activities of the overlying roof and the dense distribution of BSE. To weaken the kinetic energy released by roof breakage during the "square" period, before excavation, a special relief measure of roof deep hole blasting pressure was implemented towards the solid coal side and the goaf 0251 side within 105 m of the chute ahead of the panel (Zone B in Figure 8(n)). The specific parameters are as follows: the spacing of 10 m, the depth of 36 m, and the charge weight of 85 kg. In contrast, thanks to the pressure-relief measure for the roof adopted in the chute in advance, the distribution of the BSE near the chute

is relatively stable during excavation. And the relatively dangerous position is the middle area of the panel where the roof is not managed (d-B). As shown in Figures 8(e)–8(h), at this stage, Panel 0250 is above the underlying goaf 0290, and the overburden structure is damaged due to the caved zone and fractured zone formed by the excavation of No. 9 coal seam. First, the ranges of overburden fracture and slip during No. 5 coal seam excavation greatly narrow, and the concentration of stress and abutment pressure is effectively controlled. Second, the loose and broken coal and rock structure raise the attenuation coefficient of vibration wave propagation, and the vibration energy is significantly weakened. Therefore, at this stage, the BSE and burst hazard near the panel tend to stabilize, which indicates that the excavation of the lower protective layer has played a good effect of "load reduction-vibration reduction-energy absorption". As shown in Figures 8(i)–8(m), at this time, Panel 0250 is near the stopping line, and the advance abutment stress of the panel is superimposed with the high static load stress caused by the dense roadways on the northwest side, resulting in high concentration of BSE and high burst hazard, which is basically consistent with the zones of strong burst hazard that were previously determined by active SVT technology. Before excavation, a special pressure relief measure of large-diameter drilling was taken on the coal on both sides of the roadway within 125 m of the air duct ahead of the panel (Zone C in Figure 8(n)). The construction parameters are identical with those of Zone A. At this stage, the distribution of BSE inside the panel is relatively stable, and the
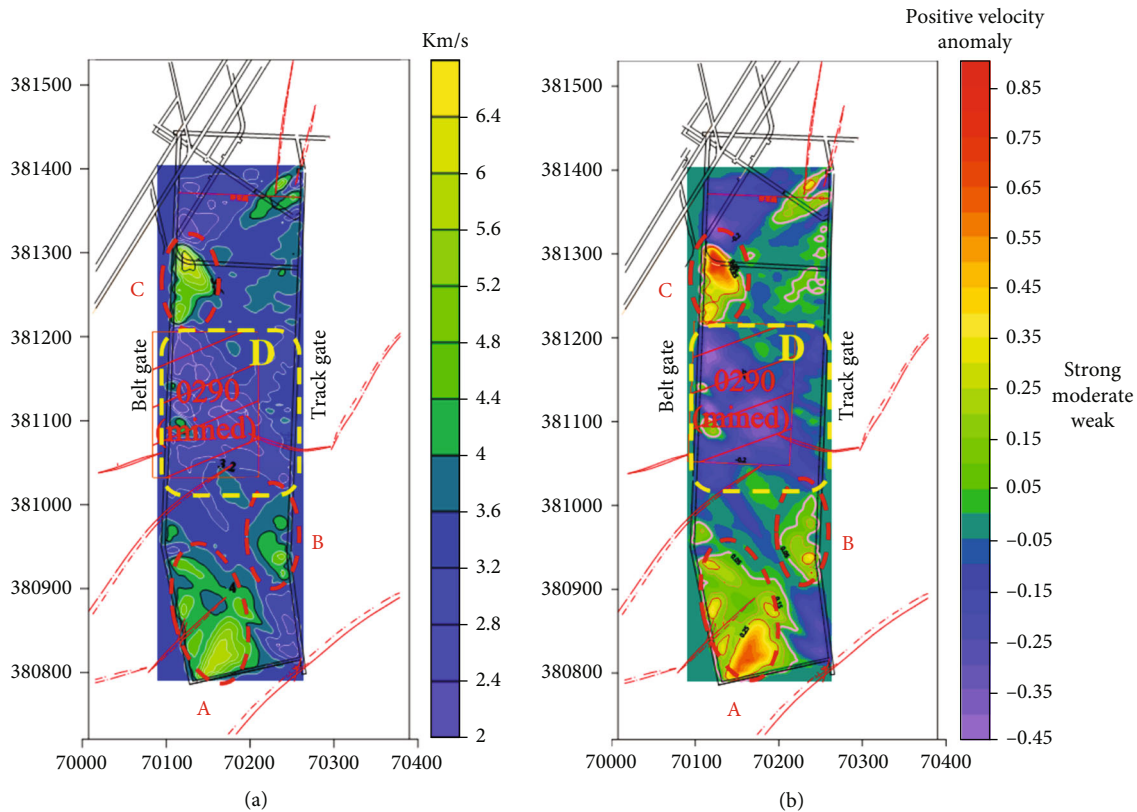
FIGURE 7: Diagrams of P-wave distribution and velocity anomaly inversion. (a) Wave velocity distribution result. (b) Velocity anomaly inversion result.

concentrated positions are mainly the dense cross roadway areas outside the panel (i-A-m-A). In addition, at this stage, multiple roadways in the north of Panel 0250 were excavated, resulting in significant concentration of BSE near the stopping line (e-A-h-A).

In conclusion, the results of static stress field detected based on active SVT before excavation well agree with the results of mining vibration field detected based on BSE during excavation. The active SVT technology not only reflects the positive anomaly state of stress concentration caused by fault structure, panel "square," and adjacent dense roadways, but also reveals the negative anomaly state of stress relief caused by "protective layer" mining. The reliable and accurate detection results provide a new idea for formulating reasonable pressure-relief parameters and testing the pressure relief effect.

4.3. Prediction Results of BSE. The research finds that under complex geological conditions and mining layouts, the main control factors and occurrence mechanism of coal burst are complex, and the precursory information of the incubation-triggering disaster remains unclear. Therefore, a detection method that integrates BSE and active SVT should realize both periodic qualitative detection and quantitative burst hazard evaluation of the panel. Figure 9(a) shows the burst hazard distribution determined by BSE from Nov. 1, 2020 to Nov. 31, 2020. The red marks are the microseismic events from Dec. 1, 2020 to Dec. 31, 2020; and the yellow one is a

strong seismic event near the stopping line of Panel 0250 on Dec. 18, which released 6.5×10^5 J energy (Figures 9(b) and 9(c)). The strong seismic event caused local roof caving ahead of the air duct and block ejection on sides in local connecting roadway, and it was felt by workers. Figure 9(d) shows the evolution of BSE index of the panel in the time domain.

According to Figure 9(a), the anomaly area of BSE from Nov. 1 to Nov. 31, 2020 is the area where microseismic events are centralized before the "12.18" strong seismic event, and the strong seismic event occurred in the corresponding high burst hazard area. This indicates that the location of potential high-hazard seismic event of the working face in the next mining stage can be roughly determined based on active SVT technology and BSE index, which can guide timely pressure-relief measures. According to Figure 9(d), almost all the main shocks (dangerous seismic events) occur when the BSE index is greater than or equal to 0.75, i.e., the corresponding burst hazard is above the moderate level. Especially before the "12.18" strong seismic event, the BSE index remained at a strong burst hazard level. Two dangerous seismic events occurred successively one day before the occurrence of strong seismic event, indicating that the BSE index can also play a good prediction effect in terms of the time domain of burst hazard.

To sum up, considering the occurrence of strong seismic events like the "12.18" seismic event, it is necessary to detect the static stress field in the mining area with the aid of active
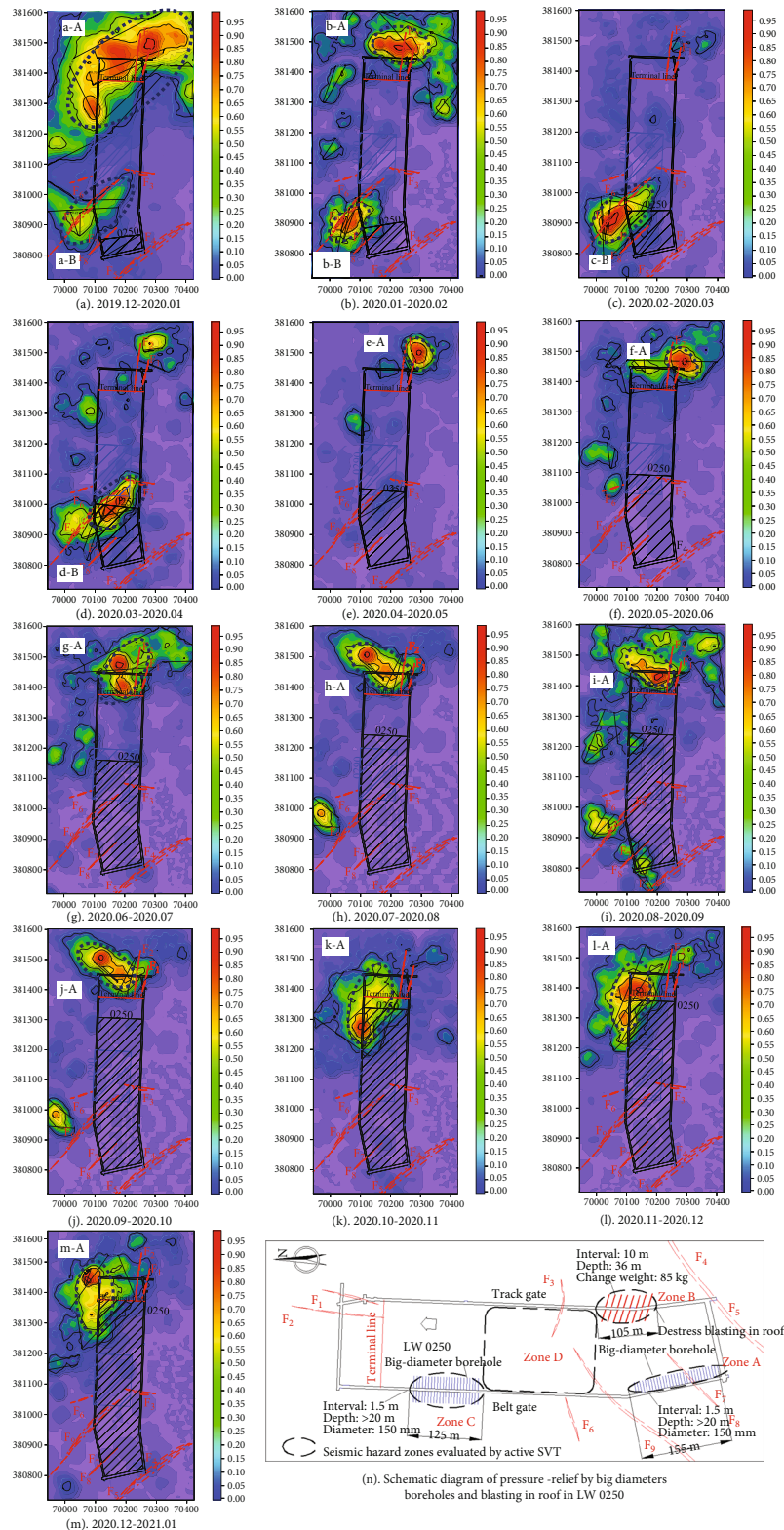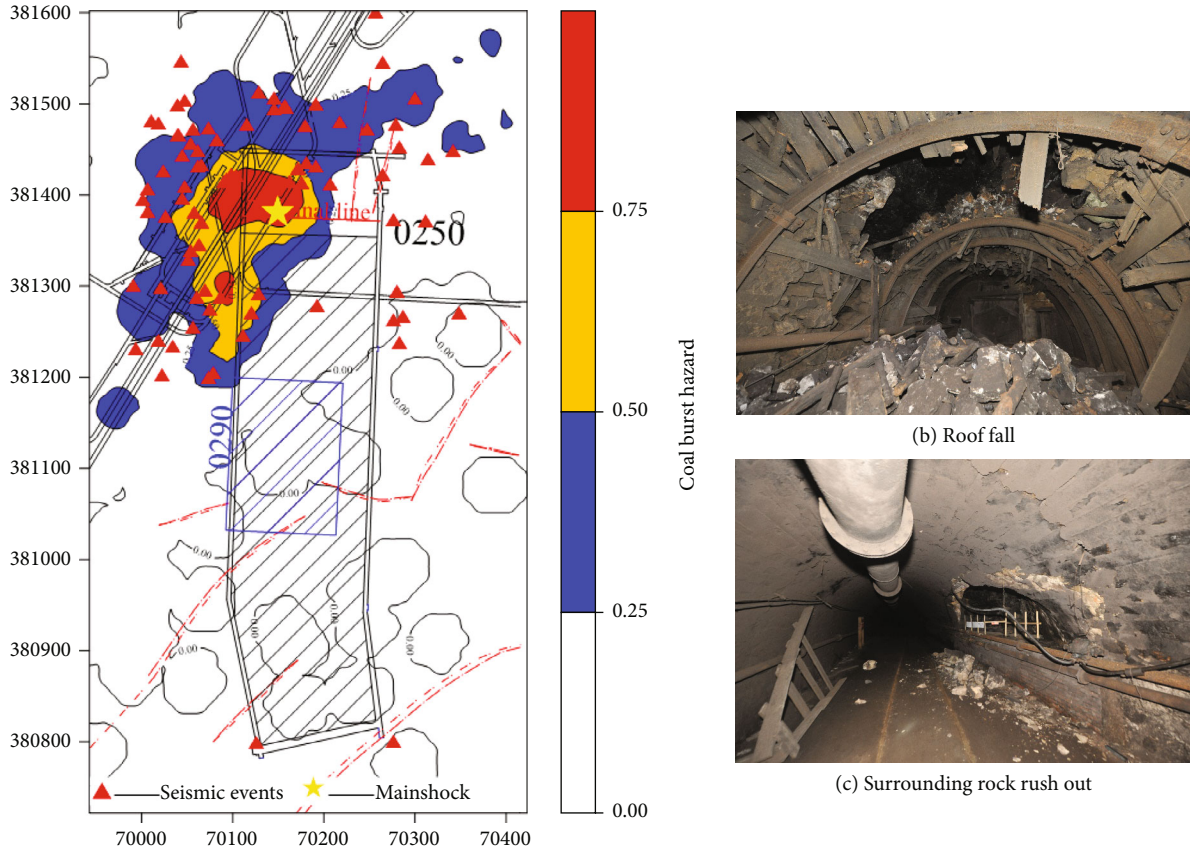
FIGURE 8: Maps of the BSE index.

SVT technology in the early stage of excavation. The real-time burst hazard state and hazard level of local locations in time and space domains need to be determined with the aid of BSE index driven by theory and data during mining.

Finally, the area and time with potential bursts can be determined based on the detection results. This can help to take reasonable targeted pressure-relief measures to ensure the safety of the working face excavation.
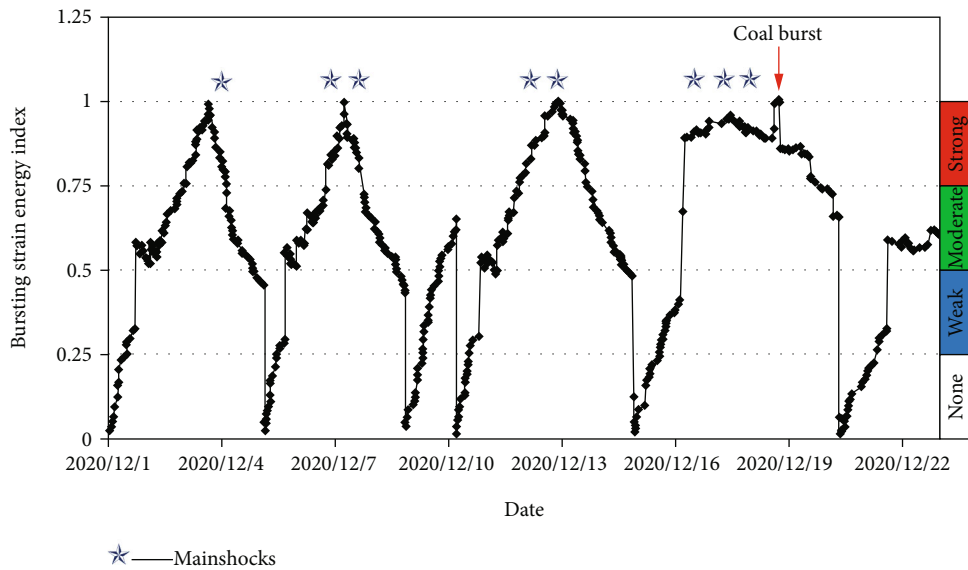
(b) Roof fall

(c) Surrounding rock rush out

(a) Plan views of the spatial distribution of seismic events (from 1 Nov. to 31 Nov. 2020) and bursting strain energy index (from 1 Dec. to 31 Dec. 2020)

(d)) Evolution of the BSE index

Figure 9: (a) Plan views of the spatial distribution of seismic events (from 1 Nov. to 31 Nov. 2020) and bursting strain energy index (from 1 Dec. to 31 Dec. 2020); (b) and (c) destroyed area of the coal burst occurring on Dec. 18, 2020; (d) evolution of the BSE index.

5. Conclusions

In this study, the whole evolution process of coal burst induced by dynamic and static loads was expounded first. On this basis, an integrated detection technology that inte-grates the BSE index and the active SVT technology was proposed. Furthermore, the burst hazard was assessed by taking the whole excavation process of a deep panel under complex conditions as the object. The main conclusions are as follows:

(1) The evolution process of coal burst in coal mines under the superposition of dynamic and static loads can be divided into four stages, i.e., incubation-triggering-appearance-end, which suggests that the occurrence of coal burst is closely related to the stress field and energy field of the mining space of coal and rock. The monitoring and early warning of coal burst hazard in the mining space should also be conducted from the perspectives of stress and energy

(2) The active SVT technology can not only identify the positive anomaly state of stress concentration caused by fault structure, panel "square," and adjacent dense roadways, but also reflect the negative anomaly state of stress relief caused by the mining of the upper protective layer. This technology can serve as a reliable method to detect the regional stress field before excavation

(3) The BSE index can not only determine the occurrence time of potential strong seismic events in the time domain, but also accurately evaluate the burst hazard level and state of local areas. It can regularly and effectively detect the coal burst risk in the excavation process

Data Availability

The data used to support the findings of this study are available from authors.

Conflicts of Interest

The authors declare that there is no conflict of interests regarding the publication of this paper.

Acknowledgments

References

[1] C. G. Zhang, I. Canbulat, B. Hebblewhite, and C. Ward, "Assessing coal burst phenomena in mining and insights into directions for future research," *International Journal of Coal Geology*, vol. 179, pp. 28–44, 2017.

[2] A. Mazaira and P. Konicek, "Intense rockburst impacts in deep underground construction and their prevention," *Canadian Geotechnical Journal*, vol. 52, no. 10, pp. 1426–1439, 2015.

[3] J. Zhou, X. B. Li, and H. S. Mitri, "Evaluation method of rockburst: state-of-the-art literature review," *Tunnelling and Underground Space Technology*, vol. 81, pp. 632–659, 2018.

[4] Y. D. Jiang, Y. X. Zhao, H. W. Wang, and J. Zhu, "A review of mechanism and prevention technologies of coal bumps in China," *Journal of Rock Mechanics and Geotechnical Engineering*, vol. 9, no. 1, pp. 180–194, 2017.

[5] S. F. Wang, L. Q. Huang, and X. B. Li, "Analysis of rockburst triggered by hard rock fragmentation using a conical pick under high uniaxial stress," *Tunnelling and Underground Space Technology*, vol. 96, article 103195, 2020.

[6] C. Srinivasan, S. K. Arora, and R. K. Yaji, "Use of mining and seismological parameters as premonitors of rockbursts," *International Journal of Rock Mechanics and Mining Sciences*, vol. 34, no. 6, pp. 1001–1008, 1997.

[7] B. Gutenberg and C. F. Richter, "Frequency of earthquakes in California∗," *Bulletin of Seismological Society of America*, vol. 34, no. 4, pp. 185–188, 1944.

[8] L. J. Dong, L. Y. Zhang, H. N. Liu, K. Du, and X. L. Liu, "Acoustic emission b value characteristics of granite under true triaxial stress," *Mathematics*, vol. 10, no. 3, p. 451, 2022.

[9] A. Y. Cao, L. M. Dou, W. Cai, S. Y. Gong, S. Liu, and G. C. Jing, "Case study of seismic hazard assessment in underground coal mining using passive tomography," *International Journal of Rock Mechanics and Mining Sciences*, vol. 78, pp. 1–9, 2015.

[10] W. Cai, L. M. Dou, A. Y. Cao, S. Y. Gong, and Z. L. Li, "Application of seismic velocity tomography in underground coal mines: a case study of Yima mining area, Henan, China," *Journal of Applied Geophysics*, vol. 109, pp. 140–149, 2014.

[11] S. Q. He, D. Z. Song, Z. L. Li et al., "Precursor of spatio-temporal evolution law of MS and AE activities for rock burst warning in steeply inclined and extremely thick coal seams under caving mining conditions," *Rock Mechanics and Rock Engineering*, vol. 52, no. 7, pp. 2415–2435, 2019.

[12] T. B. Zhao, Y. C. Yin, and Y. L. Tan, "Safe mining and new prediction model in coal seam with rock burst induced by roof," *Disaster Advances*, vol. 5, no. 4, pp. 961–965, 2012.

[13] L. W. Zhang, X. Y. Zhang, J. Wu, D. K. Zhao, and H. Fu, "Rockburst prediction model based on comprehensive weight and extension methods and its engineering application," *Bulletin of Engineering Geology and the Environment*, vol. 79, no. 9, pp. 4891–4903, 2020.

[14] W. Cai, M. D. Lin, G. Y. Si et al., "A new seismic-based strain energy methodology for coal burst forecasting in underground coal mines," *International Journal of Rock Mechanics and Mining Sciences*, vol. 123, article 104086, 2019.

[15] W. Cai, L. M. Dou, S. Y. Gong, Z. L. Li, and S. S. Yuan, "Quantitative analysis of seismic velocity tomography in rock burst hazard assessment," *Nature Hazards*, vol. 75, no. 3, pp. 2453–2465, 2015.

[16] G. N. Feit, O. N. Malinnikova, V. S. Zykov, and V. A. Rudakov, "Prediction of rockburst and sudden outburst hazard on the basis of estimate of rock-mass energy," *Journal of Mining Science*, vol. 38, no. 1, pp. 61–63, 2002.

[17] Z. L. Mu, J. Yang, G. J. Liu, Y. C. Zhang, and J. H. Jiao, "Investigation on mechanism of coal burst induced by the geological weak surface slip in coal seam bifurcation area: a case study in Zhaolou coal mine, China," *Lithosphere*, vol. 2022, no. Special 11, article 6780739, 2022.

[18] W. Cai, L. M. Dou, S. Y. Gong, A. Y. Cao, J. He, and S. Liu, "A principal component analysis/fuzzy comprehensive evaluation model for coal burst liability assessment," *International Journal of Rock Mechanics and Mining Sciences*, vol. 81, pp. 62–69, 2016.

[19] Z. L. Mu, G. J. Liu, J. Yang et al., "Theoretical and numerical investigations of floor dynamic rupture: a case study in Zhaolou Coal Mine, China," *Safety Science*, vol. 114, pp. 1–11, 2019.

[20] C. B. Wang, A. Y. Cao, C. G. Zhang, and I. Canbulat, "A new method to assess coal burst risks using dynamic and static loading analysis," *Rock Mechanics and Rock Engineering*, vol. 53, no. 3, pp. 1113–1128, 2020.

[21] Z. L. Mu, J. Yang, J. H. Jiao et al., "Application of strong pressure relief technology in deep isolated working face," *Coal Science and Technology*, vol. 42, no. 2, pp. 10–23, 2021.

[22] J. Z. Bai, L. M. Dou, J. Z. Li, K. Y. Zhou, J. R. Cao, and J. L. Kan, "Mechanism of coal burst triggered by mining-induced fault slip under high-stress conditions: a case study," *Frontiers in Earth Science*, vol. 10, article 884974, 2022.

[23] S. F. Wang, Y. Tang, and S. Y. Wang, "Influence of brittleness and confining stress on rock cuttability based on rock indentation tests," *Journal of Central South University*, vol. 28, no. 9, pp. 2786–2800, 2021.

[24] Z. L. Zhou, X. B. Li, X. Cai, W. Z. Cao, and X. M. Du, "Dynamic response and energy evolution of sandstone under coupled static–dynamic compression: insights from experimental study into deep rock engineering applications," *Rock Mechanics and Rock Engineering*, vol. 53, no. 3, pp. 1305–1331, 2020.

[25] H. P. Xie, C. B. Li, M. Z. Gao, R. Zhang, F. Gao, and J. B. Zhu, "Conceptualization and preliminary research on deep in situ rock mechanics," *Chinese Journal of Rock Mechanics and Engineering*, vol. 40, pp. 217–232, 2021.

[26] K. Luxbacher, E. Westman, P. Swanson, and M. Karfakis, "Three-dimensional time-lapse velocity tomography of an underground longwall panel," *International Journal of Rock Mechanics and Mining Sciences*, vol. 45, no. 4, pp. 478–485, 2008.

[27] N. Hosseini, K. Oraee, K. Shahria, and K. Goshtasbi, "Studying the stress redistribution around the longwall mining panel using passive seismic velocity tomography and geostatistical estimation," *Arabian Journal of Geosciences*, vol. 6, no. 5, pp. 1407–1416, 2013.

[28] S. C. Maxwell and R. P. Young, "A comparison between controlled source and passive source seismic velocity images," *Bulletin of Seismological Society of America*, vol. 83, no. 6, pp. 1813–1834, 1993.

[29] E. C. Westman, K. Luxbacher, and S. Schafrik, "Passive seismic tomography for three-dimensional time-lapse imaging of mining-induced rock mass changes," *The Leading Edge*, vol. 31, no. 3, pp. 338–345, 2012.

[30] P. Banka and A. Jaworski, "Possibility of more precise analytical prediction of rock mass energy changes with the use of passive seismic tomography readings," *Archives of Mining Sciences*, vol. 55, no. 4, pp. 723–731, 2010.

[31] D. F. Scott, J. M. Girard, T. J. Williams, and D. K. Denton, "Comparison of Seismic Tomography, Strain Relief, and Ultrasonic Velocity Measurements to Evaluate Stress in an Underground Pillar," in *Proceedings of society for mining metallurgy and exploration annual meeting*, Denver, 1999.

[32] J. G. Gibowicz and A. Kijko, *An Introduction to Mining Seismology*, Academic Press, London, 1994.

[33] N. Hosseini, K. Oraee, K. Shahriar, and K. Goshtasbi, "Passive seismic velocity tomography on longwall mining panel based on simultaneous iterative reconstructive technique (SIRT)," *Journal of Central South University*, vol. 19, no. 8, pp. 2297–2306, 2012.

[34] L. H. Tan, Z. L. Zhou, X. Cai, and Y. C. Rui, "Analysis of mechanical behaviour and fracture interaction of multi-hole rock mass with DIC measurement," *Measurement*, vol. 191, article 110794, 2022.

[35] S. Wang, L. Sun, X. Li et al., "Experimental investigation of cuttability improvement for hard rock fragmentation using conical cutter," *Internal Journal of Geomechanics*, vol. 21, no. 2, 2021.

[36] H. Benioff, B. Gutenberg, and C. F. Richter, "Progress Report, Seismological Laboratory, California Institute of Technology, 1950," *Transactions of the American Geophysical Union*, vol. 32, no. 5, p. 749, 1951.